Rheol Acta (2012) 51:609–621
DOI 10.1007/s00397-012-0635-9

ORIGINAL CONTRIBUTION

Shear-dependent thermal conductivity of alumina nanofluids

Seokwon Kim · Chongyoup Kim · Wook-Hyun Lee · Seong-Ryong Park

Received: 23 November 2011 / Revised: 8 April 2012 / Accepted: 11 April 2012 / Published online: 17 May 2012

Abstract The thermal conductivities (k) of aqueous alumina nanofluids of various particle shapes (rods, bricks, blades) were measured at the dynamic state for the first time. The dynamic k was measured under torsional flows by using a homemade parallel-plate system. The homemade system was validated by numerical simulations and experiments with homogeneous liquids. All the nanofluids tested here showed decreasing k with increasing shear rate. This newly observed phenomenon was named 'shear-reducing thermal conductivity.' The dispersion characteristics were characterized by the dynamic light scattering (DLS) and rheological techniques. From the rheological properties of nanofluids it was inferred that the alumina nanofluids should have network structures and these microstructures should be destroyed or deformed by shearing. But not all the networks were destroyed by shearing. The DLS data revealed that some nanoparticles in nanofluids should exist as individual particles. The effective medium theory cannot explain the shear-reducing characteristics of nanofluids at the dynamic state. The rheological data imply that the heat percolation through the network may not be the sole reason for heat transfer enhancement in nanofluids. It is suggested that the Brownian motion of the primary particles cannot be excluded in heat conduction through nanofluids.

Keywords Shear-reducing thermal conductivity · Viscosity · Elasticity · Gel · Network · Brownian motion

S. Kim · C. Kim (✉)
Department of Chemical and Biological Engineering, Korea University, Anam-dong, Sungbuk-ku, Seoul 136-713, Korea
e-mail: cykim@grtrkr.korea.ac.kr

W.-H. Lee · S.-R. Park
Korea Institute of Energy Research, 102 Gajeong-ro, Jang-dong, Yoosung-ku, Daejeon 305-343, Korea

Introduction

Nanofluid is a heat transfer fluid in which nanoparticles are suspended in a conventional heat transfer fluid. The earlier works for nanofluids have concentrated primarily on the thermal properties of materials after Choi and Eastman (1995) presented the thermal conductivity enhancement. During the last several years, the heat transfer enhancement has been explained by Maxwell Garnett (1904) model that is based on the effective medium theory and the Hamilton and Crosser (1962) model that is an extension of the Maxwell model considering the effect of non-spherical particle shape. In addition, the effects of heat percolation through aggregation (Xuan et al. 2003; Prasher et al. 2006; Evans et al. 2006) and micro-convection induced by Brownian motion (Jang and Choi 2004; Prasher et al. 2005) on thermal conduction have been investigated. Also, there has been a controversy over the contribution of Brownian motion (Keblinski et al. 2002). In fact, the heat transfer experiments were not reproducible even though the same materials were used. There were large differences among the measured values and the models, which is possibly due to the different dispersion statuses and preparing methods of nanofluids (Buongiorno et al. 2009). Until now no generic theory has yet been found

to explain the thermal conductivity enhancement of nanofluids.

Nanofluids are colloidal suspensions. A nanofluid may have a larger viscosity than fluids dispersed with micron-sized particles due to the increase in effective volume fraction induced by the electrical double layer around the particles. In some cases, shear-thinning viscosities are observed due to changes in microstructure and reduced Brownian motions. Generally, rheological characteristics can vary depending on size and shape of particles. Non-spherical particles can be oriented by flow field producing a stronger elastic effect when compared with the spherical one. However, non-Brownian characteristics are expected if the aspect ratio is much larger than 10 (Larson 1999). Severely shear-thinning viscosity and the increase of the zero-shear viscosity are likely to be observed with increasing aspect ratio (Brenner 1974). Moreover, not only the viscosity but also the viscoelastic properties are strongly affected by the excluded volume due to the rotation of non-spherical particles.

The state of dispersion is influenced by size, shape, volume fraction and electrostatic characteristics of particles. The electrostatic force provides the repulsion force and the particles do not aggregate when the repulsion is strong enough. On the other hand, particles can be aggregated or become networked by attractive forces. The van der Waals attraction among particles can be controlled by adjusting pH or concentration of electrolyte (or salt). Both of colloidal and non-colloidal suspensions could undergo a fluid-to-solid transition due to the formation of disordered (fractal) structure, and the transition status can be quantified by viscosity and/or elasticity. Trappe et al. (2001) have suggested a phase diagram among particle volume fraction (Φ), inter-particle attractive energy (U) and applied shear stress for attractive colloidal particles. It has been shown that there are two extreme cases of hard-sphere colloidal particles at high Φ and low U and attractive (soft) particles at low Φ and high U. In the case of hard-sphere colloidal particles at high Φ and low U, a fluid-to-glass transition could occur near the crowded (particle) packing fraction (Trappe et al. 2001; Trappe and Sandkuhler 2004; Mason and Weitz 1995). On the other hand, for attractive particles at low Φ and high U, a sol-to-gel transition could take place at low particle volume fraction and form a space-filling percolating network showing $G' > G''$ and a plateau G' at low frequency (Trappe et al. 2001; Segre et al. 2001). To describe the status of dispersion, the scale of aggregate can be defined by the fractal theory and estimated by the viscosity measurement of the suspension (Larson 1999; Chevaler et al. 2009). In the case of rodlike particles, a gel structure can be formed easily when increasing the aspect ratio of the particle. Also non-polar particles that have a strongly attractive force can readily undergo a fluid–solid transition in contrast with the polar particles (Mobuchon et al. 2009).

In our recent study on the nanofluid at the equilibrium state, we observed that $G' > G''$ at all frequencies when the cylinder-shaped alumina particles were dispersed in water and Φ was larger than 0.03 (Kim et al. 2011). In addition, a plateau in G' occurred at the low frequency regime. This is a typical gel behavior in that a network cannot be destroyed easily by an applied shear stress and subsequently exhibits a stress-bearing structure, in other words, the network would not be easily destroyed by stress (Trappe et al. 2001; Segre et al. 2001). Furthermore, the four orders of magnitude increase in viscosity was observed compared with the viscosity of water. The increase in viscosity strongly implies that spanning-networks should be formed (Larson 1999). But some small particles or flocs should exist that are not bound to the network and therefore free to move. This argument will be supported by the dynamic light scattering (DLS) study on particle size distribution in the present study. Therefore, the alumina nanofluid should be considered as a weakly flocculated gel, where the networked/aggregated particles coexist with the individual ones. Kim et al. (2011) also showed that thermal conductivity decreased dramatically when the weakly flocculated gel was transformed to a strongly flocculated gel by pH adjustment. The decrease in k with the large increase in viscosity strongly implies that the Brown motion of particle plays an important role in the thermal conductivity enhancement.

Conventional heat transfer fluids such as water and ethylene glycol are homogeneous fluids and have constant properties under the flow condition both thermally and rheologically. On the other hand, nanofluids may not have the same properties. This is because physical properties can be influenced by the microstructure developed in the fluid. Also, the flow can suppress the Brownian motion of particles which may be one of the key factors for heat transfer enhancement as discussed above. Ahuja (1975) found that the thermal conductivity of suspensions under laminar flow is about three times larger than the thermal conductivity of stationary suspensions of 50 or 100 μm spherical polystyrene beads under tube flows. In this case, the Brownian motion should be negligible since the particle size is large. But the measurement of k by a tube flow have difficulties since the velocity and particle concentration profiles are not uniform due to the migration of particles to low shear regions (Han et al. 1999). Sohn and Chen (1984) carried out analytical researches to

find out the flow dependency on thermal conductivity by using a power-law model fluid under the uniform heat flux and wall temperature conditions and showed that the thermal conductivity increased with shear-rate above the threshold. Shin and Lee (2000) prepared suspensions of polyethylene beads of 25, 100, 180, and 300 μm in a mixture of silicone oil and kerosene and measured the thermal conductivity under the flow condition using Couette geometry. The particle concentration was in the range of $0 < \Phi < 0.10$. They found that, at the rest state, the thermal conductivity enhancement was not significantly large and was independent of particle size. This was because the difference in the thermal conductivity between the particle and the liquid was small (the thermal conductivity of the polymer particle is 0.45 W/m·K and those of silicon oil and kerosene are 0.164 W/m·K and 0.150 W/m·K, respectively). However, the thermal conductivity increased with shear-rate when particle size was larger than 25 μm. Moreover, the shear-rate dependency became stronger when particle size became larger. It appears that the micro scale convection induced by particles at the high shear-rate regime induces the stronger dependency. This can be surmised from the fact that the particles move more affinely with the flow when particles are smaller and the larger particles induce a larger convection effect due to larger difference in relative velocity between particle and fluid.

Until now, there have been no reports on the physical properties of nanofluid under flow conditions. To utilize a nanofluid as a heat transfer fluid, it is certain that its rheological and thermal properties should be characterized also under the flow condition for the better design of a flow system. In this paper, the thermal conductivity of alumina nanofluids has been investigated while changing shear-rate expecting a greater extent of enhancement when compared with the suspensions containing micron-sized polymer particles. We prepared nanofluids by dispersing nanometer-sized alumina particles of short rod, blade, brick, or long rod (Timofeeva et al. 2009) shape in water and measured the thermal conductivities at different shear-rates while comparing with the value at the stationary state. We have found that the k decreases with increase in shear rate. The reduction in thermal conductivity appears to be caused at least partially by the suppressed Brownian motion by the flow. The magnitude of increase in k here may be not large enough for practical purpose. In the present research, we have tried to resolve the controversy over the heat transfer enhancement mechanism by applying the rheological methodology. Understanding the enhancement mechanism will shed light on the design of practically usable nanofluid.

Experiments

Materials and particle size measurements

Four different types of non-spherical alumina particles were dispersed in deionized water. The volumetric concentrations (Φ) were 0.01, 0.03, and 0.05. One rod type (short rod hereafter) alumina was purchased from Sigma-Aldrich and brick, blade, and another rod type (long rod hereafter) alumina were donated from North American Sasol Company. Their average particle sizes and shapes are listed in Table 1. The particles obtained from Sasol Co. contain less than 2 % of nitric, acetic and formic acids. Therefore, their aqueous suspensions were acidic and pH value was 4 approximately. The acids can stabilize the alumina suspension electrostatically since they do not adsorb chemically onto the particle surface and also can release ions in water to increase the surface charge. For this reason, stable nanofluids of non-spherical nanoparticles can be obtained simply by mixing with water since pH of the suspension is much lower than the IEP (isoelectric point) of alumina of 8–9. The pH of the aqueous suspension of alumina particles obtained from Aldrich Co. was approximately 8–9 and therefore the pH was adjusted to 5 by adding 3.0 M HCl aqueous solution in order to achieve electrostatic stabilization. To prepare a suspension, alumina powders were mixed with 500 ml of deionized water in a beaker first. Then the mixture was agitated for 3 h using a magnetic stirrer (Corning Laboratory Stirrer/Hot Plate PC620) with a magnetic bar of 45 mm in diameter. The stirring speed was maintained so that the vortex touched the bottom of the beaker. The suspension was then left for 24 h without any further treatment. Before measuring properties, the sample was sonicated.

Table 1 Size and shape of alumina particle: primary particle size by TEM and dispersed size by DLS

	Short rod (nm)	Blade (nm)	Brick (nm)	Long rod (nm)
Primary particle size from TEM images	<50	10/60	40	10/50
Average particle size by DLS	250	200	90	90

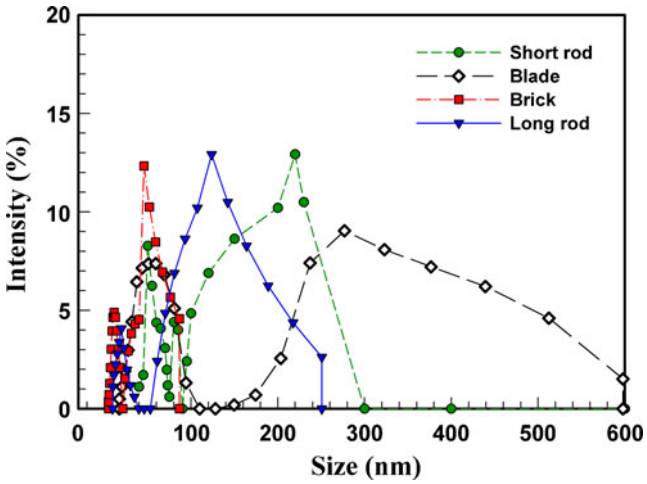

Fig. 1 Particle (or aggregate) size distribution measured by DLS

The size of dispersed particles (or aggregates) was investigated first since thermal and rheological properties can vary with size and shape of the primary particles. The dynamic light scattering (DLS) technique (Brookhaven Goniometer, BI-200SM) was used to measure particle size and its distribution in the diluted state. The fitting function was the CONTIN provided by the manufacturer. In Fig. 1 and Table 1 the average particle sizes and the particle (or aggregate) size distributions measured by DLS are compared with the electron microscopy images shown in Fig. 2. In all cases, single particles are observed as well as aggregates. In the case of blades, large aggregates coexist with primary particles. The aggregate size of bricks is much smaller than the blade aggregates.

Rheological measurements

Rheological properties of nanofluids were measured using a stress-controlled rotational rheometer (AR2000, TA Instruments) with the Couette geometry (inner diameter of 14 mm, outer diameter of 15 mm). Viscosity was measured as a function of shear-rate and G' and G'' were measured as a function of frequency after the linear viscoelastic regime was confirmed by strain sweep tests. To minimize the effect of different

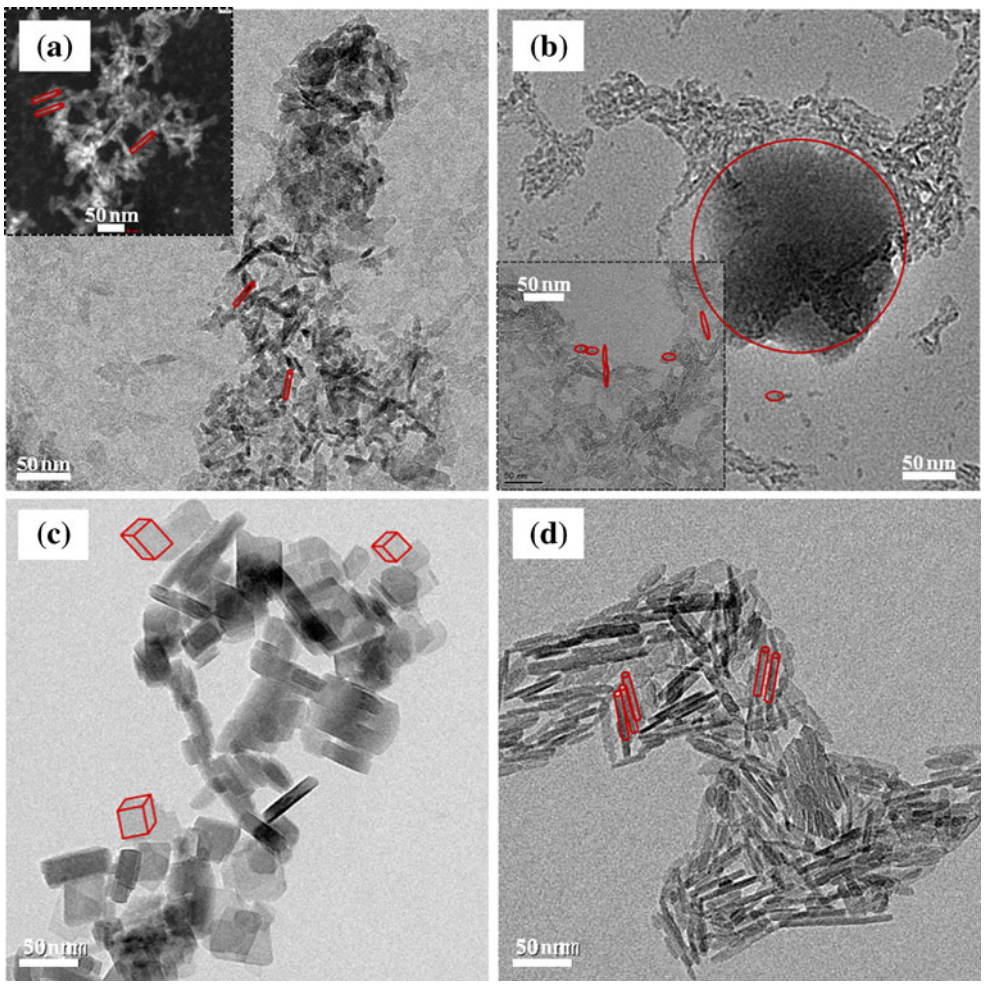

Fig. 2 TEM images of nanoparticles: **a** short rod; **b** blade; **c** brick; **d** long rod

aging times for different samples, the measurement was started by waiting for 1 h without stirring after sonication for 120 min (750 W, 20 % amplitude and 20 kHz). The sampling time was maintained for 3 min to reach the equilibrium by avoiding fluctuations which appeared when the equilibrium was not reached especially in the case of an attractive system. When the sampling time was longer than 3 min the results were almost independent of sampling time, while fluctuations appeared if sampling time was shorter than 3 min.

Thermal conductivity under flow by parallel-plate system

To measure thermal conductivity under shearing conditions, a parallel-plate system was designed in which a rotating circular plate was placed between two fixed circular plates as shown in Fig. 3. The diameters of the stationary and rotating plates were 110 and 100 mm, respectively. The gap distance between the stationary and rotating plates was fixed at 1 mm. A rubber area-heater was placed on the top of the upper plate in order to apply a constant heat flux. To the bottom of the lower plate, five thermoelectric chips (Thermo-electric chip, Thermotron Inc, 30 mm × 30 mm × 3.8 mm, Q_{max} = 33.2 W × 5) with fins and a fan were attached to keep the lower plate at a constant temperature. A DC power supply (Agilent, E3611A) was used for the area-heater. To confirm temperature uniformity, temperatures were measured at three radially different positions using K-type thermocouples that were inserted into the holes drilled to 500 μm from the liquid surface at the upper

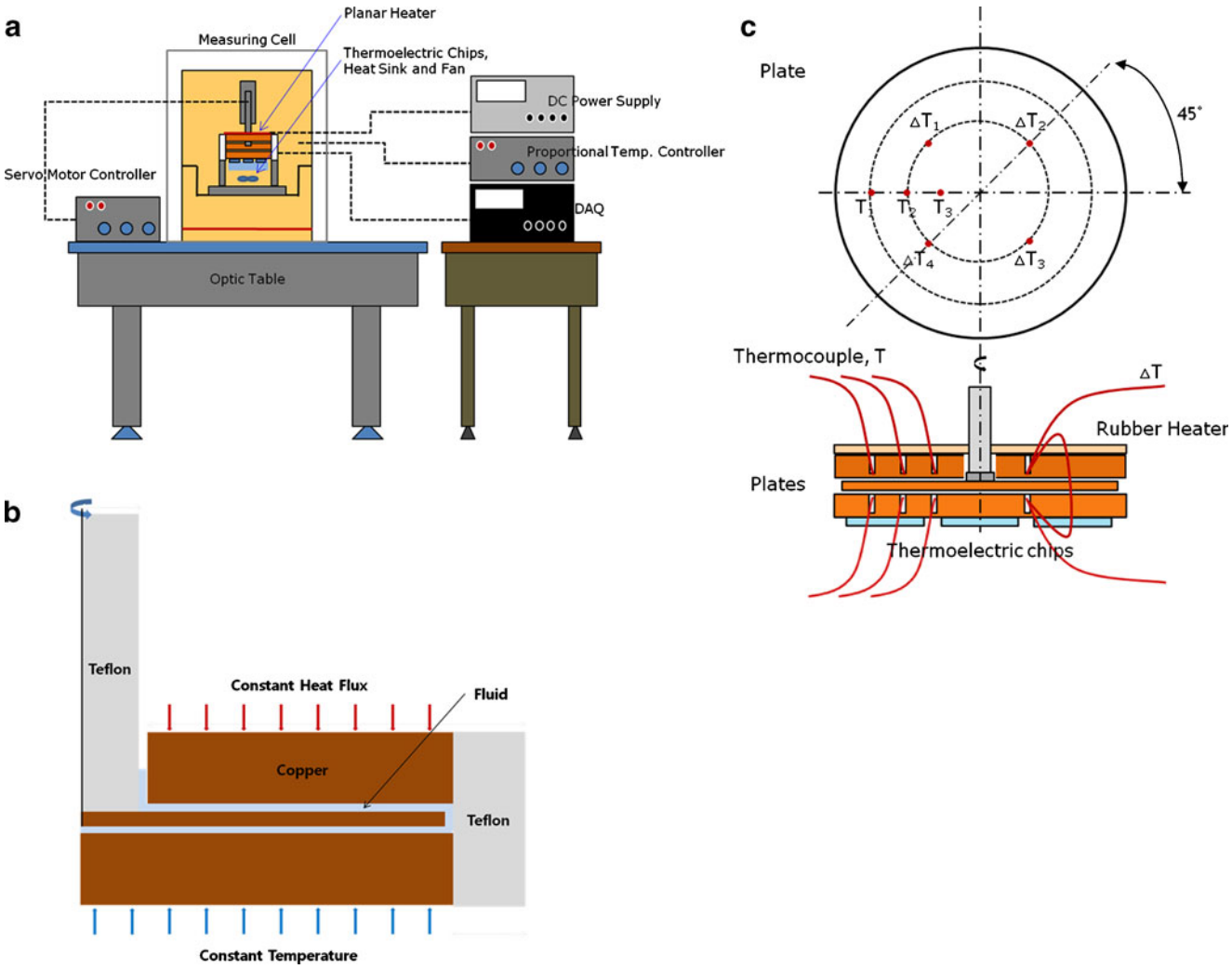

Fig. 3 Schematic diagrams of the experimental apparatus for measuring k under dynamic conditions: **a** system configuration; **b** parallel-plate system. The diameters of the stationary and rotating plates are 110 and 100 mm, respectively; **c** positions of thermocouples for temperature and temperature difference measurements. Thermocouples for measuring the plate temperature ($T_i, i = 1, 2, 3$) were placed radially with 10 mm spacing. Thermocouple junctions for measuring the temperature difference (ΔT_i, $i = 1$–4) were positioned at the radial distance of 20 mm with 90° spacing

and lower plates. These thermocouples were used for checking the temperature uniformity only. The temperature difference between the two plates was measured using a multi-junction thermocouple for more accurate measurements (Rohsenow et al. 1985). Four junctions were placed at each plate as shown in Fig. 3c and the temperature difference was calculated from the average electromotive force. The junctions were inserted into the holes drilled to 500 μm from the liquid surface as described before. The thermocouples were connected to a data acquisition system (Agilent, 34970A). The middle plate was connected to a servo motor (Mitsubishi, KFS13, 100 W, 3,000 rpm) to rotate while controlling the rotating speed accurately. The middle plate rotated stably by using a high-resolution encoder (131,072 pulses/revolution).

Dimensions and materials as well as the operating conditions of the parallel-plate system were selected after numerical simulations using a commercial software package (Fluent™, Ansys Inc.). The effect of forced convection and steady-state temperatures were investigated by analyzing temperature gradients, velocity gradients, and the stream functions for water and ethylene glycol for which the physical and chemical properties were well-known. First, we calculated the heat losses from the upper plate, lower plate, insulating wall, interface between fluid and air and rotating axis when they were made from stainless steel and the gap distance was 1.0 mm. When the constant heat flux was applied, temperature gradients existed in both the axial and radial directions for the stainless steel plates. However, temperature gradients in both directions disappeared if the plates were made of copper so that the effect of convection in the system could be neglected. The effect of convection at the edge of the rotating plate was studied by observing the swirl velocity and stream function. It was found that convective motions were too strong at the edge of the parallel plates when the rotor speed was over 10 rpm. Therefore the maximum rotational speed was set to 5 rpm in the experiments which corresponds to 13 s^{-1} in the average shear rate. In the test runs with water, the measured thermal conductivity differed about 20–30 % from the reference value when 0.10–3.00 W of heat was applied. The large difference appeared to be due to temperature fluctuations. Small fluctuations in temperature could lead to a large error when the applied heat was small and particularly if the insulating part had a large ρC_p. As a consequence, the steady-state temperature could not be reached easily. Fortunately, the error was reduced within 10 % when the applied heat was 4.5 W. To reduce the heat loss by convection between the system and the external environment, the measuring system was placed in an environment chamber the temperature of which was controlled by a proportional controller for fine control. The temperature fluctuation was within ±0.40 K when the environmental temperature was higher than 30°C, but it decreased to ±0.10 K when 4.0 W was applied and the external temperature was 27°C. The calculated thermal conductivity value had less than ±4.0 % error from the reference value when the fluctuation was within ±0.15 K. One drop of silicon oil which had a smaller density than water and did not mix with water was added to the interface between the fluid and the air formed around the rotor shaft to prevent evaporation of water from the nanofluid. A quasi-steady state reached after the heat flux was applied over 2 h. When the rotating speed was smaller than 10 rpm the secondary flow was found to be virtually suppressed between parallel plates based on the simulation study.

Results and discussion

Aggregate size and its distribution

Aggregates, the average diameter of which is two to seven times larger than the primary particle, are identified from the particle size measurement by DLS. Since the shape of the particles (or aggregates) cannot be determined by this method only, we referred to the transmission electron microscopic data. In Figs. 1 and 2, blades and cylinders have almost the same aspect ratio of 5–6. In addition, the particle size distribution by DLS shows the coexistence of aggregates and primary particles. Since the samples for DLS study are diluted from the concentrated nanofluid to avoid multiple scattering we may not argue that the primary particles exist in the same proportion in the concentrated system. However it is certain that some primary particles should exist even in aggregated nanofluids since we did not impose any strong shear during the dilution stage and in this case the proportion of the primary particles may not be much different even though the microstructure of the aggregates may be changed slightly. The presence of primary particles implies that Brownian motions of the primary particles cannot be neglected in the enhancement of thermal conductivity even in the case of aggregated suspensions. The existence of non-breakable flocs appears to be in agreement with literatures. It has been reported that the flocs of cylindrical particles are much more difficult to break compared with flocs of spherical particles (Mohraz and Solomon 2005). Also it has been reported that even flocs of latex particles as large as 380 nm in diameter cannot be broken under the shear rate of 80 s^{-1} in water (Selomulya et al. 2001).

Since the particles used here have much smaller sizes and cylindrical, blade or brick shapes, it is surmised that the flocs was not broken. So even if the arrangement of particles and flocs can occur during shear, the complete deflocculation of the aggregated particles is not expected in our system.

Thermal conductivity

In this section, we consider the thermal conductivity of alumina nanofluids under shearing conditions. Then, we will consider the rheological properties of nanofluid to probe the microstructure of nanofluid and will seek possible connections between the thermal conductivity and the microstructure. Before describing these properties here, we briefly consider the errors in measuring k at the dynamic state. There should be many factors which affect the accuracy of measurements. Among these heat loss appears to be most significantly affecting. Heat could be lost by thermal conduction through the walls and the main shaft which holds the rotating plate and the evaporation of fluid at the liquid–air interface. If heat is lost, the temperature difference between the two stationary plates reads smaller than the true value and the calculated k will then be larger than the true value. Another important factor is the secondary flows which are developed between the stationary and rotating plates by the inertia of fluid. To determine the proper operating condition with negligible secondary flow effects, we performed numerical simulations using the Fluent software. Our equipment was designed in such a way that the temperature difference was measured to calculate k by the following equation while supplying a constant heat flux Q.

$$k = \frac{Q}{\pi R^2 (T_{\text{upper}} - T_{\text{lower}})/2d} \tag{1}$$

In the above equation, R is radius of the plate, d is the gap distance between the stationary, and moving plates and T is temperature. Also, the subscripts *upper* and

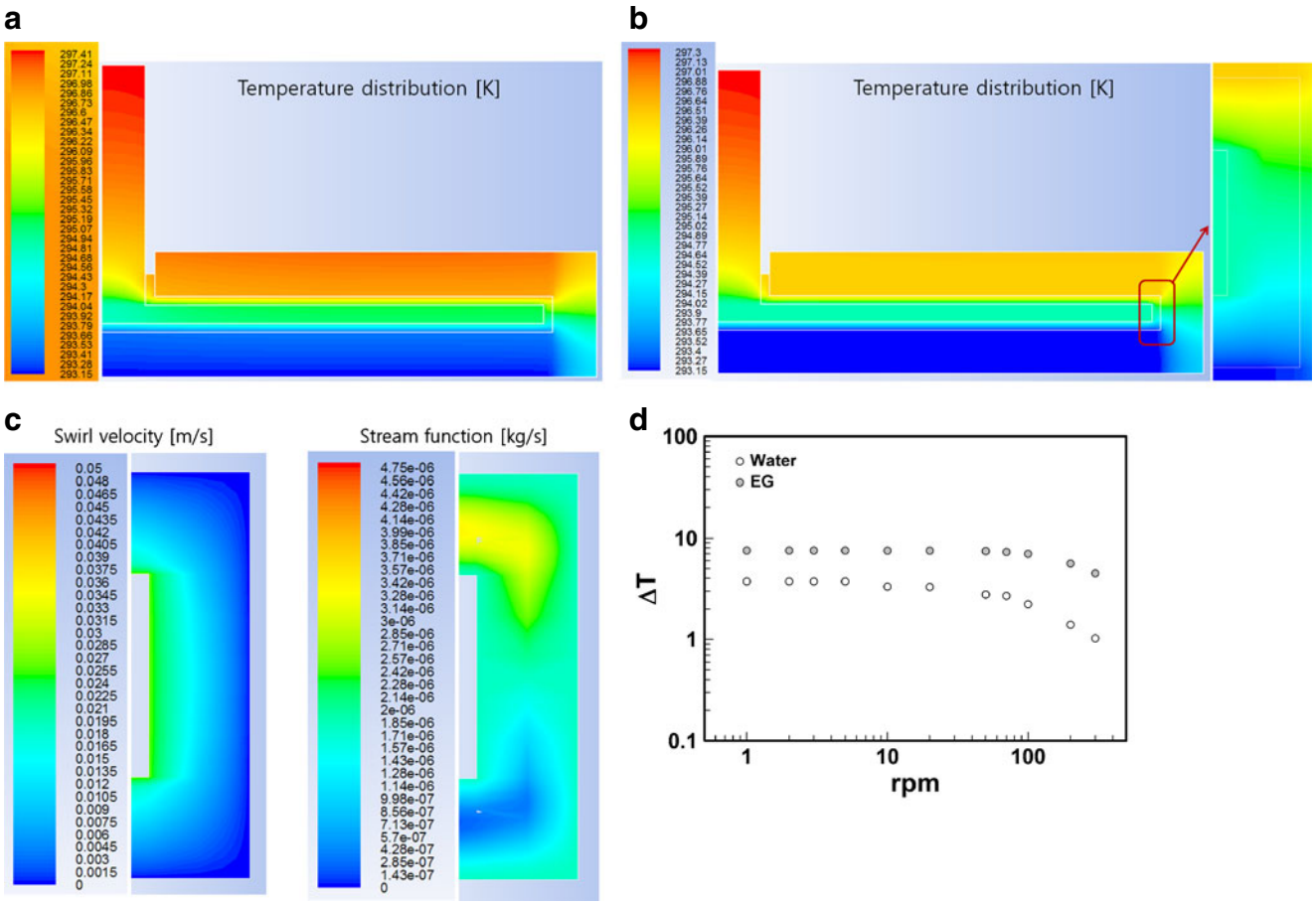

Fig. 4 Temperature distributions and flow patterns in the parallel plate system estimated by numerical simulations when the gap distance is 1 mm. **a** Plates made of stainless steel; **b** plates made of copper; **c** flow characteristics near the edge of the rotating plate: *left* Swirl velocity; *right* stream function; **d** rotating speed (rpm) vs. temperature difference

lower denote the upper and lower fixed plates, respectively. If a strong secondary flow exists, the convective heat transfer cannot be neglected and the apparent k will be higher. Experimentally, the measured temperature difference will be smaller than the value with negligible secondary flows under a fixed heat flux condition. Since the secondary flow is caused by the inertial effect it will become stronger with rotation speed. In Fig. 4d, we have plotted the simulation results on the temperature difference with rotation speed for water and ethylene glycol. From the figure we can confirm that the temperature differences, hence the thermal conductivities, are not affected by the rotation if it is less than 5 rpm for water and it is as large as 30 rpm for ethylene glycol. Therefore we restricted the rotational speed to 5 rpm in the experiment. This rotational speed corresponds to the maximum shear rate of 26 s^{-1} at the edge of the plate.

To estimate the overall measurement error of our set-up, we first measured k's of water and ethylene glycol at the dynamic state as well as at the static state and found that k of water and ethylene glycol had the values of 0.64 ± 0.03 and 0.27 ± 0.02 W/m·K, respectively, when a constant heat flux of 4.5 W was applied for 12 h. Hence the maximum relative error was 5 and 7 %, respectively. Also the k values at the dynamic state were the same as the static values as expected for homogenous fluids. This means that the accuracy of the dynamic measurement is the same as the static measurement, and therefore any differences in measured k values between the static and dynamic states of nanofluids can be regarded to be caused by the shear flow along the azimuthal direction without being affected by the secondary flow in radial and axial directions. Since the primary purpose of the present study was to compare the dynamic k value with the static one, we did not regard the seemingly large error of 5 % as serious one.

In measuring k of a suspension, some important issues should be considered which do not appear in the case of homogeneous fluids. These are the slip layer, settling and particle migration. The slip can be caused by two major reasons of the geometric exclusion of particles from the wall and particle migration by hydrodynamic interaction between particles. Therefore, particle migration can be an issue only for dilute systems for which particles or aggregates are not in networks. In the present case, the particle migration by particle–particle interactions can be excluded since the hydrodynamic diffusion coefficient $D_{\text{hydro}} \approx \dot{\gamma} a^2 = 1.5 \times 10^{-15} \text{m}^2\text{s}^{-1}$ is much smaller than the Brownian diffusivity $\left(D_{\text{Brown}} = \frac{kT}{6\pi\eta a} \approx 2.5 \times 10^{-11} \text{m}^2\text{s}^{-1}\right)$ for particles of 20 nm dispersed in water at 300 K and shear rate of 15 s^{-1}. Here, we assumed that particles are spherical since no general theory is given yet on the hydrodynamic diffusion of non-spherical particles. For aggregates of 200 nm in diameter, these are 1.5×10^{-13} and 2.5×10^{-12} m^2 s^{-1}, respectively. Therefore, the Brownian diffusion is still much stronger than the hydrodynamic diffusion even for aggregated particles. The slip layer caused by the geometric exclusion is usually one or two diameters of particle thick. This means that the thickness is far less than 1 μm. Since the thickness of the fluid layer (1 mm) is at least 1,000 times the slip layer thickness, the contribution of the slip layer should be negligibly small considering that k can be written as follows:

$$\frac{d}{k} = \frac{d - 2l_{\text{slip}}}{k_1} + \frac{2l_{\text{slip}}}{k_{\text{solvent}}} \tag{2}$$

In the above equation k_1 is k of the suspension excluding the slip layer, l_{slip} the slip layer thickness and d is the gap distance between plates. Since $l_{\text{slip}}/d \approx 10^{-4}$ and k_1 is not that large compared with the pure fluid, k of nanofluid is not affected by the slip layer to a meaningful amount. In the present experiment, there was no settling of particles or aggregates of the nanofluid made from Sasol alumina. This was confirmed by Turbiscan data for a 24-h period as shown in Fig. 5. Actually there was no settling of nanoparticles in the nanofluids stored for several months. The issue related with sedimentation of particles will be reconsidered.

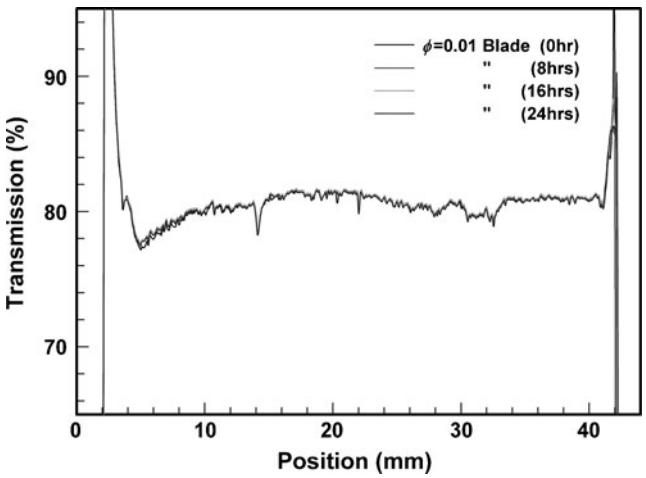

Fig. 5 Settling stability of nanofluids (transmission (%) vs. position with time by Turbiscan). This sample has the lowest viscosity among the samples we tested hence the sample is most prone to sedimentation. The profiles are indistinguishable since there is almost no sedimentation during the 24-h period. The peak at 1 mm is due to the bottom of the glass vial containing the sample and the peak at 41 mm is due to the meniscus at the air–nanofluid interface. The experiment was performed at 293 K

In Fig. 6, thermal conductivities of alumina nanofluids measured at the dynamic and static states are compared. First of all, it is noted that k decreases with shear rate regardless of particle shape and particle loading. We will call this newly observed phenomenon 'shear-reducing thermal conductivity'. We may argue that the increased k of the nanofluid over k of the pure fluid at the static state should be caused by a mechanism which becomes weaker with increasing shear rate. This point will be considered later when we consider the rheological properties. The reduction in k is larger for more concentrated nanofluid. In the case of nanofluid of short rods, k at the dynamic state becomes virtually the same as k of the pure liquid when shear rate is 13 s^{-1}. One may argue that k of nanofluid should be larger than that of pure liquid even at the dynamic state. It appears to be caused by the Kapitza resistance (Wilson et al. 2002; Ge et al. 2004; Nan et al. 1997) which may be large enough to compensate the small increase in k at high shear rates. The amount of increase in k varies slightly for different particle shapes and sizes.

Before describing more results, we considered whether the measured dynamic k was affected by sedimentation or aging. To check this, we first measured k at a high shear rate after a long time shearing. We chose two cases of the highest and lowest particle loadings. Then we decreased shear rate stepwise and measured k at each step. Finally we suddenly increased shear rate to the initial value and checked whether k returned to the initial value sufficiently closely. As shown in Fig. 7, k varied reversibly when shear rate changed. The series of experiments shows that there was no settlement of particles and the subsequent concentration of particles at the center. Also, the dynamic k was not affected by aging.

In Fig. 8a, viscosity (η) and storage and loss moduli (G' and G'') of the nanofluid of short rods are plotted. In the figure the viscosity of nanofluid when $\Phi = 0.01$ is almost the same as that of water, but the viscosity

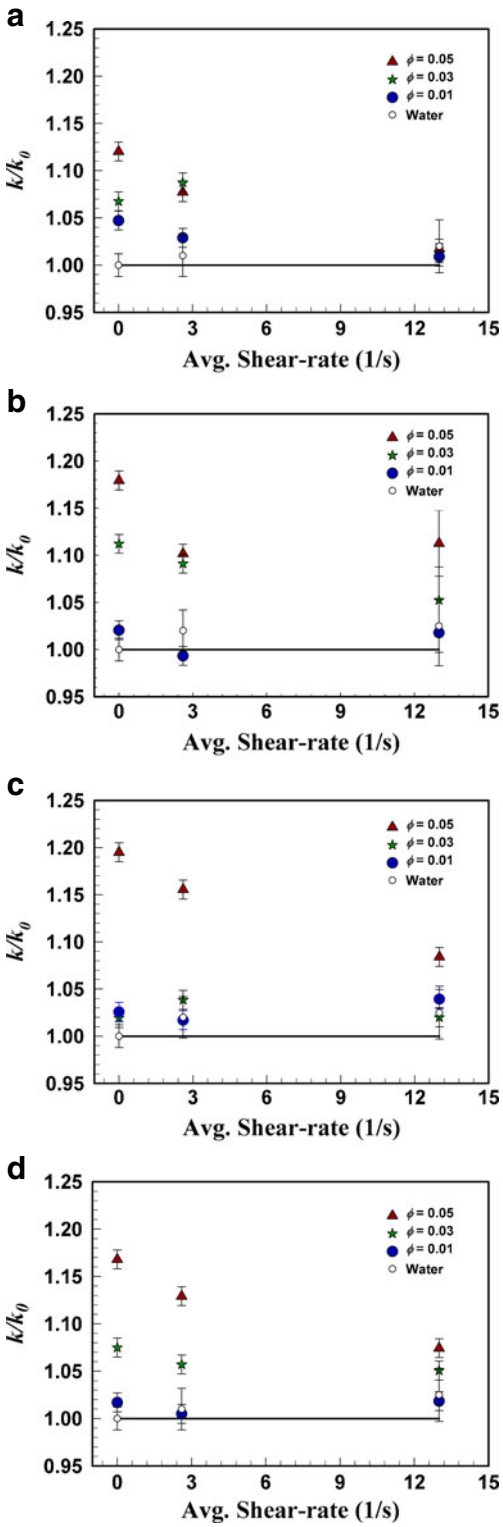

Fig. 6 The ratio of the thermal conductivities between nanofluid and its base fluid (water) as a function of average shear rate: **a** short rod; **b** blade; **c** brick; **d** long rod

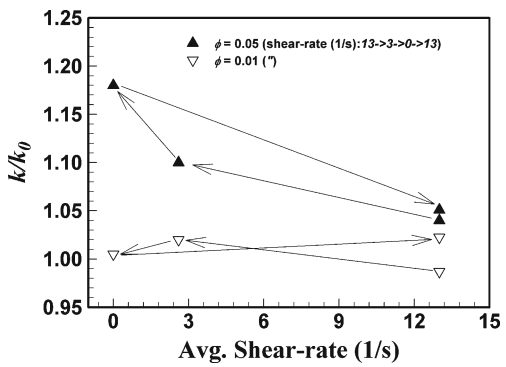

Fig. 7 Reversibility of thermal conductivity when shear rate is changed after long time shearing. The thermal conductivity returns to the initial value within the experimental error

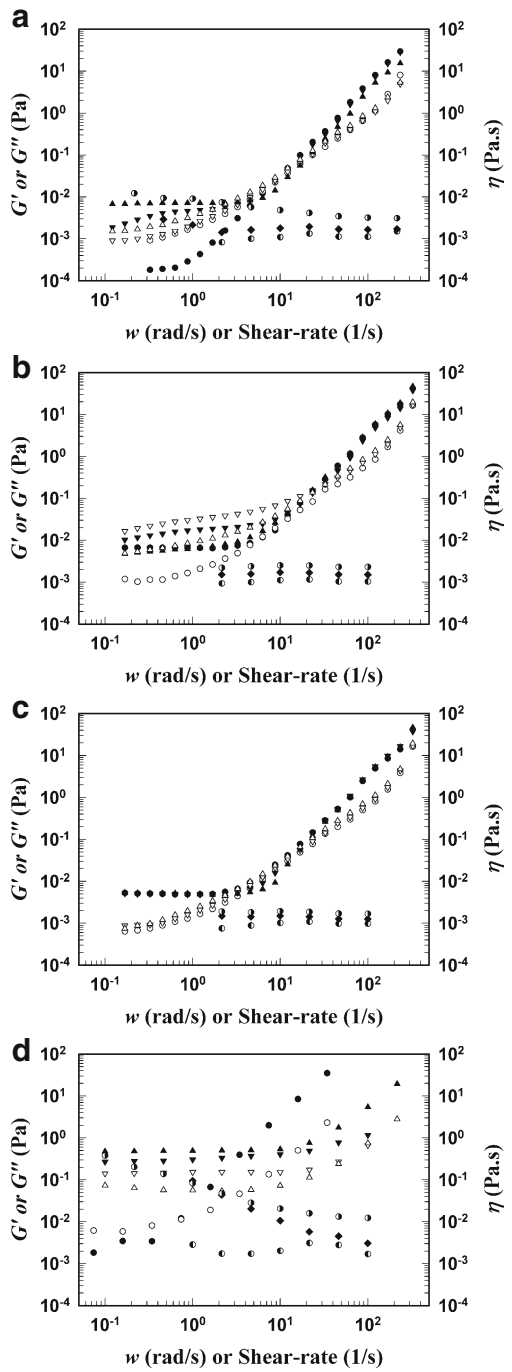

Fig. 8 Linear viscoelasticity and shear viscosity of nanofluids: **a** short rod; **b** blade; **c** brick; **d** long rod. *Symbols*: *filled circle* (G', $\Phi = 0.01$); *open circle* (G'', $\Phi = 0.01$); *filled inverted triangle* (G', $\Phi = 0.03$); *open inverted triangle* (G'', $\Phi = 0.03$); *filled upright triangle* (G', $\Phi = 0.05$); *open upright triangle* (G'', $\Phi = 0.05$); *circle with left half black* (η, $\Phi = 0.01$); *filled diamond* (η, $\Phi = 0.03$); *circle with right half black* (η, $\Phi = 0.05$)

of the nanofluid when $\Phi = 0.05$ is shear-thinning and the zero-shear viscosity of the nanofluid is about ten times larger than that of water. This means that as particle concentration becomes large there develops a microstructure due to strong particle–particle interactions among particles. The viscoelastic properties also support the formation of microstructure. When $\Phi = 0.01$, G' is much smaller than G'' at the low frequency regime ($\omega < 1\text{s}^{-1}$). The weak elasticity appears to be caused by the Brownian motion of primary particles. When $\Phi = 0.05$, G' becomes larger than G'' at the same regime and G' has a plateau when $\omega < 1$ rad/s. The plateau in G' implies that there should be a network structure within the nanofluid. The DLS data showed that the average particle size was 5 times larger than the average diameter of primary particles. Even though the DLS data cannot represent the true particle size since the nanofluid has to be diluted to measure the average particle size, it is certain that the average particle size should be at least the same as or larger than the value obtained from DLS. Therefore, the DLS data also support the existence of flocs or network structures in the nanofluid. Also there is a distribution of particle sizes in the case of short rods as shown in Fig. 1. There has been a report that polydisperse particles form aggregates easily due to the increase in the attractive force since the structure barrier among particles becomes smaller when compared with the monodisperse case (Chu et al. 1996; Richter and Gruhn 2006). Therefore, the present experimental findings described above and an independent study on polydisperse suspensions suggest a development of network structures or aggregates in alumina nanofluid when $\Phi = 0.05$. When a shear stress is applied to the nanofluid, the microstructure will be changed at least partially as manifested in the shear-thinning viscosity. Also, the Brownian motion of individual particles will be hindered by the shear stress as described below. The reduction in k at the dynamic state appears to be affected by these two factors. The effective medium theory cannot account for the reduction in k at the dynamic state since the theory is basically an equilibrium theory (Nan et al. 1997). This means that the effective medium theory cannot be a proper candidate for explaining the heat conduction in nanofluids.

Under shearing conditions particles become aligned or clustered. For example, cylindrical particles can get aligned along the flow direction. Even if this alignment can be destroyed by the Brownian motion and the Jefferey orbit, there is an average particle direction depending on shear stress. This means that particle motions under the shearing condition will not be the same as the random motion at the equilibrium state. According to the Phung and Brady's Stokesian dynamic simulation the Brownian contribution to the viscosity of a suspension of hard spheres is shear-thinning (Phung et al. 1996). The reduced contribution is due to the

increased hydrodynamic interaction between particles. This means that, even if the fluctuating Brownian force is the same, the particle motion or the size of the fluctuations is not the same. Phung and Brady's numerical work was done only on the hard-sphere case. But the core idea should be the same for non-spherical particles. That is, under the shearing condition, both the translational and rotational Brownian motions are reduced and this reduced Brownian motion may result in the reduced k at the dynamic state. The reduced Brownian motion of rod particles in suspensions will be considered in the following.

In Fig. 8b–d, rheological properties of blade, brick and rod suspensions from Sasol Co. are shown. Suspensions of different particle shapes have different rheological properties as expected. For example, the long rod suspensions show strongly shear-thinning behavior. For brick and blade suspensions, the low shear viscosities were very small and hence could not be measured due to the mechanical limit of the rheometer. Even though there are differences among different particle shapes, all the data show that G's have significantly large values, which implies that network structures be developed within the suspensions. The small viscosity of short rod, brick, or blade suspensions at high shear rates means that the network structures are fragile and hence at high shear rate the structures are destroyed by the shear. In the case of long rod suspensions, the viscosity of 5 % suspension is strongly shear-thinning and the viscosity value does not become close to the pure water value. In other words the viscosity of 5 % rod suspension does not show the full destruction of the network structure at high shear rates (over 100 s^{-1}). However, k value still becomes smaller with the increase in shear rate as shown in Fig. 6. For all cases, as described above, k value decreases with shear rate regardless of the destruction of network structures. This strongly implies that the percolation of heat through the network structure may not be the major reason for the enhancement of k in nanofluids.

To argue that Brownian motions are suppressed by the shearing motion from the equilibrium condition, Peclet number $\mathrm{Pe} = \dot{\gamma} L^2/D$ should be large, say $\mathrm{Pe} > 1$ (L, length of particle; D, diffusion coefficient). As the rheological data imply, a nanofluid becomes a gel when particle loading is high and it is not trivial to calculate the diffusivity of nanoparticles within the gel. Another issue should be the rotational diffusion of non-spherical particles. In the present research, we have estimated the translational diffusion coefficient using the theoretical prediction by Solomon and Spicer (2010) on the arrested cylindrical particle in the gel since the rheological data implies that the nanofluid shows a gel-like behavior. Solomon and Spicer used the method by Krall and Weitz (1998) and the data by Mohraz and Solomon (2006) for boehmite nanoparticles (aspect ratio of 4). Solomon and Spicer have shown that the diffusivity of a rod in a gel (D) is reduced from the diffusivity of a rod at infinite dilution (D_0) and $D/D_0 \approx 10^{-5} \sim 10^{-4}$ when the aspect ratio is 4 and particle loading has an order of 0.001. Since they did not calculate beyond this value, we assume that $D/D_0 \approx 10^{-5}$ for the nanofluids of cylindrical nanoparticles. The diffusivity at the infinite dilution is given in Doi and Edwards (1986) as follows:

$$D_0 = \frac{\ln(L/b)}{3\pi\eta_s L} k_B T \tag{3}$$

In the above equation L and b are the length and diameter of a nanoparticle, respectively, η_s is solvent viscosity, k_B is the Boltzmann constant and T is temperature. When the parameter values of the nanofluid (L, 50 nm; b, 10 nm; η_s, 0.89 mPa s; T, 300 K) are inserted, $D \approx 1.6 \times 10^{-16}$ m^2 s^{-1}. Then $\mathrm{Pe} \approx 16 > 1$ when $\dot{\gamma} = 1$ s^{-1}. Hence, the Brownian effect should be suppressed by shearing at this low shear rate. The rotational diffusivity of a nanoparticle at infinite dilution is (Doi and Edwards 1986)

$$D_{r0} = \frac{3(\ln(L/b) - \gamma)}{\pi\eta_s L^3} k_B T \tag{4}$$

where $\gamma = 0.577\cdots$ is the Euler constant. Peclet number based on the rotational diffusion coefficient is then $\mathrm{Pe_r} = \dot{\gamma}/D_r$ and has the same order of magnitude as the translational case. In actual case due to the difference in constant (3 rather than 1/3 and the Euler constant), the rotational Pe will be slightly smaller than the translational Pe. Still the rotational Brownian motion should be suppressed by shearing. In the case of blades, one may assume that their behavior should resemble the motion of rods since the ratio of the largest axis to the middle axis is 6 as listed in Table 1. In the case of blades, particles can have lamellar structures and then the movement of the particles in the lamellar structure is even more restricted. This means that Pe should be even lower and the Brownian motion is suppressed at a lower shear rate than the case of rods. Recently, Kleshchanok et al. (2012) and Constantin et al. (2010) reported that the diffusivity of platelets in suspensions is lowered by as much as three orders of magnitude. Especially the diffusivity can be lowered even in the sol state. Since the particles and liquids they used are different from ours, the physics and chemistry should be different and hence their results cannot be directly applied to our system. However, it can be inferred that the diffusivity of blades in suspensions should

be additionally lowered from their values of rods in suspensions. As far as the authors are aware of, the diffusivity of bricks has not been reported yet even in the infinite dilution case. Therefore, it is not possible to calculate its diffusivity in suspension even qualitatively. However, as seen from Fig. 2, bricks become chained by the strong interaction between faces. This means that the suspension is strongly affected by shear as bricks behave as long rods, and hence shear-reducing thermal conductivity can be observed. Therefore, the argument that the thermal conductivity is reduced by the suppressed Brownian motion can be justified.

Since the discovery of nanofluid, the mechanism of k enhancement has been controversial among nanofluid research groups. Based on the present research, we may argue that Brownian effect should be the dominant mechanism for the enhancement: The effective medium theory does not contain the particle size effect. Considering that the k enhancement is observed only for nanoparticle suspensions, the effective medium theory cannot support the experimental observations in the literature even if the model could predict reasonably the same as the experimental observation. Also the effective medium theory is an equilibrium theory hence the shear rate-dependent k cannot be explained. This is the limitation of the effective medium theory. It has been reported that when the Brownian motion is suppressed by changing pH there was almost no enhancement (Kim et al. 2011). In this case, the nanofluid became a strongly flocculated gel. This means that the percolation cannot be the sole reason for the enhancement since the percolation structure should remain in the gel. Then the Brownian mechanism remains as the candidate and the present experimental result does not have a conflict when we assume that the reduced Brownian effect is at least partially responsible for the enhancement.

In assessing the effect of Brownian motion, we should note that the Brownian "diffusion" of particles may not increase the thermal conductivity of the suspension due to the following reason. In the case of alumina particles of 50 nm (d), for example, the time to reach the thermal equilibrium (d^2/α) has an order of 2×10^{-10} s and hence particles will lose or gain the heat to and from the surrounding fluid almost instantaneously. Therefore the particles will be in the thermal equilibrium with the surrounding fluid, and there will be negligible heat transfer enhancement due to the diffusion. Also, since the thermal mass of a nanoparticle is small compared with the surrounding fluid due to its small heat capacity and size, the heat which a nanoparticle can carry with cannot be significant especially in nanofluids with low particle loadings. This argument suggests that the enhancement of Brownian "motion" should come from its micro-convection effect. When a particle moves within a liquid, a certain amount of the surrounding liquid will be dragged by the motion. When a temperature gradient exists within the fluid, there should be a net transfer of heat along the temperature gradient direction in addition to the conduction through the fluid and particles. The rotational Brownian motion can also transfer heat by a similar mechanism. The larger increase in thermal conductivity by non-spherical particles (Timofeeva et al. 2009) supports this mechanism.

Conclusions

In the present study, we have measured the thermal conductivity (k) of alumina nanofluid of various nanoparticle shapes (rods, bricks, blades) at dynamic states. All the nanofluids tested here show that as shear rate increases k decreases. We have named this phenomenon 'shear-reducing thermal conductivity' noting the resemblance to the shear-thinning viscosity in rheology. This is the first report on k at dynamic states. From the shear-reducing characteristics of k, we have concluded that the effective medium theory cannot explain the heat transfer enhancement of nanofluids at the dynamic state. We have also measured the rheological properties of nanofluids to probe the microstructure. The rheological properties of nanofluids show that the alumina nanofluids have network structures and these microstructures are destroyed or deformed by the shear. This implies that the network structure should have some effects on heat transfer characteristics somehow. In the case of long rod suspensions, the viscosity does not decrease to the water value at a sufficiently large shear rate even though the shear-reducing characteristics of k are much the same as other nanofluids which show strong destruction of the network structure. This implies that the heat percolation through the network may not be the sole reason for heat transfer enhancement. The dynamic light scattering data show that some nanoparticles in nanofluids exist partially as individual particles. It is noted that, with the increase in shear rate, the Brownian motion of primary particles that coexist with the network structure also suppressed by the shear stress. This strongly implies that the Brownian motion cannot be excluded in heat conduction through nanofluids.

Acknowledgements This work was supported by Energy-Resources Technology R&D Program of the Ministry of Knowledge Economy, Republic of Korea (Project No. 2008ECM11P080000).

The alumina nanoparticles were donated by Dr. Yun Chang of North American Sasol Inc.

References

Ahuja AS (1975) Augmentation of heat transport in laminar flow of polystyrene suspensions. I. Experiments and results. J Appl Phys 46:3408–3416

Brenner H (1974) Rheology of a dilute suspension of axisymmetric Brownian particles. Int J Multiphase Flow 1:195–341

Buongiorno J, Venerus DC, Prabhat N, McKrell T, Townsend J, Christianson R, Tolmachev YV, Keblinski P, Hu LW, Alvarado JL, Bang IC, Bishnoi SW, Bonetti M, Botz F, Cecere A, Chang Y, Chen G, Chen H, Chung SJ, Chyu MK, Das SK, Paola RD, Ding Y, Dubois F, Dzido G, Eapen J, Escher W, Funfschilling D, Galand Q, Gao J, Gharagozloo PE, Goodson KE, Gutierrez JG, Hong H, Horton M, Hwang KS, Iorio CS, Jang SP, Jarzebski AB, Jiang Y, Jin L, Kabelac S, Kamath A, Kedzierski MA, Kieng LG, Kim C, Kim JH, Kim S, Lee SH, Leong KC, Manna I, Michel B, Ni R, Patel HE, Philip J, Poulikakos D, Reynaud C, Savino R, Singh PK, Song P, Sundararajan T, Timofeeva E, Tritcak T, Turanov AN, Vaerenbergh SV, Wen D, Witharana S, Yang C, Yeh WH, Zhao XZ, Zhou (2009) A benchmark study on the thermal conductivity of nanofluids. J Appl Phys 106: 094312

Chevaler J, Tillement O, Ayela F (2009) Structure and rheology of SiO_2 nanoparticle suspensions under very high shear rates. Phys Rev E 80:051403

Choi SUS, Eastman JA (1995) Enhancing thermal conductivity of fluids with nanoparticles, development and application of non-Newtonian flows. ASME FED 231/MD66:99–103

Chu XL, Nikolov AD, Wasan DT (1996) Effects of particle size and polydispersity on the depletion and structural forces in colloidal dispersions. Langmuir 12:5004–5010

Constantin D, Davidson P, Freyssingeas E, Madsen A (2010) Slow dynamics of a colloidal lamellar phase. J Chem Phys 133:224902

Doi M, Edwards SF (1986) The theory of polymer dynamics. Oxford University Press

Evans W, Fish J, Keblinski P (2006) Role of Brownian motion hydrodynamics on nanofluid thermal conductivity. Appl Phys Lett 88:093116

Ge ZB, Cahill DG, Braun PV (2004) AuPd metal nanoparticles as probes of nanoscale thermal transport in aqueous solution. J Phys Chem B 108:18870–18875

Hamilton RL, Crosser OK (1962) Thermal conductivity of heterogeneous two component systems. Ind Eng Chem Fundam 1:187–191

Han M, Kim C, Kim M, Lee S (1999) Particle migration in tube flow of suspensions. J Rheol 43:1157–1174

Jang SP, Choi SUS (2004) Role of Brownian motion in the enhanced thermal conductivity of nanofluids. Appl Phys Lett 84:4316–4318

Keblinski P, Phillpot SR, Choi SUS, Eastman JA (2002) Mechanisms of heat flow in suspensions of nano-sized particles (nanofluids). J Heat Mass Transfer 45:855–863

Kim S, Kim C, Lee W, Park S (2011) Rheological properties of alumina nanofluids and their implication to the heat transfer enhancement mechanism. J Appl Phys 110:034316

Kleshchanok D, Heinen M, Nagele G, Holmqvist P (2012) Dynamics of charged gibbsite platelets in the isotropic phase. Soft Matter 8:1584–1592

Krall AH, Weitz DA (1998) Internal dynamics and elasticity of fractal colloidal gels. Phys Rev Lett 80:778–781

Larson RG (1999) The structure and rheology of complex fluids. Oxford University Press, Oxford

Mason TG, Weitz DA (1995) Linear viscoelasticity of colloidal hard sphere suspensions near the glass transition. Phys Rev Lett 75:2770–2773

Maxwell Garnett JC (1904) Colours in metal glasses and in metallic films. Philos Trans R Soc London Ser A 203:385–420

Mobuchon C, Carreau PJ, Heuzey MC (2009) Structural analysis of non-aqueous layered silicate suspensions subjected to shear flow. J Rheol 53:1025–1048

Mohraz A, Solomon MJ (2005) Orientation and rupture of fractal colloidal gels during start-up of steady shear flow. J Rheol 49:657–681

Mohraz A, Solomon MJ (2006) Gelation and internal dynamics of colloidal rod aggregates. J Colloid Interface Sci 300:155–162

Nan CW, Birringer R, Gleiter H (1997) Effective thermal conductivity of particulate composites with interfacial thermal resistance. J Appl Phys 81:6692–6699

Phung TN, Brady JF, Bossis G (1996) Stokesian dynamics simulation of Brownian suspensions, J Fluid Mech 313:181–207

Prasher P, Bhattacharya P, Phelan PE (2005) Thermal conductivity of nanoscale colloidal solutions (nanofluids). Phys Rev Lett 94:025901

Prasher R, Phelan PE, Bhattacharya P (2006) Effect of aggregation kinetics on the thermal conductivity of nanoscale colloidal solutions (nanofluid). Nano Lett 6:1529–1534

Richter A, Gruhn T (2006) Structure formation and fractionation in systems of polydisperse attractive rods. J Chem Phys 125:064908

Rohsenow WM, Hartnett JP, Ganić EN (1985) Handbook of heat transfer applications. McGraw Hill, New York

Segre PN, Prasad V, Schofield AB, Weitz DA (2001) Glasslike kinetic arrest at the colloidal-gelation transition. Phys Rev Lett 86:6042–6045

Selomulya C, Amal R, Bushell G, Waite TD (2001) Evidence of shear rate dependence on restructuring and breakup of latex aggregates. J Colloid Interface Sci 236:67–77

Shin SH, Lee SH (2000) Thermal conductivity of suspensions in shear flow fields. Int J Heat Mass Transfer 43:4275–4284

Sohn CW, Chen MM (1984) Heat transfer enhancement in laminar slurry pipe flows with power law thermal conductivities. J Heat Transfer 106:539–542

Solomon MJ, Spicer PT (2010) Microstructural regimes of colloidal rod suspensions, gels, and glasses. Soft Matter 6:1391–1400

Timofeeva EV, Routbort JL, Singh D (2009) Particle shape effects on thermophysical properties of alumina nanofluids. J Appl Phys 106:014304

Trappe V, Sandkuhler P (2004) Colloidal gels—low-density disordered solid-like states. Curr Opin Colloid Interface Sci 8:494–500

Trappe V, Prasad V, Cipelletti L, Segre PN, Weitz DA (2001) Jamming phase diagram for attractive particles. Nature (London) 411:772–775

Wilson OM, Wu X, Cahill DG, Braun PV (2002) Colloidal metal particles as probes of nanoscale thermal transport in fluids. Phys Rev B 66:224301

Xuan YM, Li Q, Hu WF (2003) Aggregation structure and thermal conductivity of nanofluids. AIChE J 49:1038–1043